Morphological effects on the transport and magnetic properties of polymeric and colloidal carbon aerogels

G. A. M. Reynolds
Department of Physics, Massachusetts Institute of Technology, Cambridge, Massachusetts 02139

A. W. P. Fung
Department of Electrical Engineering and Computer Science, Massachusetts Institute of Technology, Cambridge, Massachusetts 02139

Z. H. Wang
Francis Bitter National Magnet Laboratory, Massachusetts Institute of Technology, Cambridge, Massachusetts 02139

M. S. Dresselhaus
Department of Physics and Department of Electrical Engineering and Computer Science, Massachusetts Institute of Technology, Cambridge, Massachusetts 02139

R. W. Pekala
Department of Chemistry and Materials Science, Lawrence Livermore National Laboratory, Livermore, California 94550
(Received 27 July 1994)

The temperature-dependent conductivity, magnetoresistance, magnetic susceptibility, and room-temperature Raman scattering of carbon aerogel samples with different morphologies and various grain sizes are studied. In particular, carbon aerogels with a *polymeric* morphology are studied and compared with *colloidal* carbon aerogels. The conductivity exhibits an $\exp[-\sqrt{T_0/T}]$ dependence for all samples at low temperature. This strong localization behavior can be explained by a Coulomb-gap variable-range hopping mechanism, and this identification has been further corroborated by the low-temperature magnetoresistance data obtained in a magnetic field up to 15 T. Magnetic susceptibility measurements suggest that carbon aerogels with a smaller grain size are more disordered, in agreement with the conductivity data. The results suggest that the grains themselves, and not the defects within, act as carrier localization sites in these materials.

PACS number(s): 72.20.My, 72.80.Ng, 81.35.+k

I. INTRODUCTION

Carbon aerogels are a special type of low-density microcellular material (LDMM).[1] The LDMM's combine the low densities of materials, such as polystyrene foams, with the ultrafine pore sizes of membranes. The organic carbon aerogels studied in this work are derived from the highly polymerized resorcinol-formaldehyde (RF) aerogel.[1,2] The structure and properties of these RF aerogels can be chemically tailored on a nanometer scale to generate materials with low densities (0.03–0.6 g/cm^3), high porosities ($> 75\%$), and large specific surface areas (400–1000 m^2/g). The resultant carbon aerogels obtained from pyrolysis of the RF aerogel retain these features, giving rise to a unique material in terms of its possible commercial applications and structure-property relationships.[2–4]

The microstructure of carbon aerogels consists primarily of interconnected carbon grains (particles). Inside these grains is a network of intertwined graphitic filaments of width $\sim$ 30 Å. The interconnectivity and the size of the grains are dependent on the molar ratio of resorcinol to catalyst (i.e., Na_2CO_3) (R/C) used during the RF aerogel synthesis. Under high catalyst concentration conditions, well-connected *polymeric* RF aerogels are formed (grain size 30–60 Å), while low catalyst concentrations result in *colloidal* RF aerogels with grains connected in a "string-of-pearls" configuration (grain diameter 120–300 Å).[1,5] After pyrolysis the grain sizes change, as will be seen below.

Previous studies on colloidal carbon aerogels[6] suggest that the primary electrical conduction mechanism is most likely associated with the grain interconnectivity, rather than with the disorder internal to the grains. Other studies show that heat treatment tends to partially graphitize these materials, increasing their conductivity.[7,8] The present study investigates the effects of changing the grain size and the microstructural morphology on the transport mechanisms. Our present data suggest that the previously observed[9] Coulomb-gap variable-range hopping (CGVRH) (Ref. 10) conduction mechanism remains valid despite variations in the grain size and the granular shape. Also, our data confirm that the grains, rather than the dangling bonds present in the system, act as carrier localization sites in these carbon aerogel monoliths.

In this paper, a brief description of the different aero-

gel microstructures studied is given in Sec. II. The experimental procedures are presented in Sec. III, while Sec. IV gives a synopsis of the experimental results obtained from Raman spectroscopy, magnetic susceptibility, electrical conductivity, and magnetoresistance measurements. Sec. V discusses our results as they pertain to the CGVRH theory, while Sec. VI presents our conclusions.

II. AEROGEL MICROSTRUCTURE

Before discussing the issue of structural characterization of carbon aerogels, it is instructive to understand the structural differences between colloidal and polymeric aerogels. Figure 1 shows the high-resolution TEM micrographs of these two types of aerogels. Generally, both classes of aerogels consist of grains with micropores between connected grains as well as inside the grains. In addition, mesopores are formed between chains of interconnected grains. The grains consist of a network of intertwined carbon filaments or ribbons. The grain connectivity and the RF network vary for the two aerogel types. By increasing the packing ratio of the grains, the mass density of the carbon aerogel can be increased.

For colloidal carbon aerogels (low catalyst ratio, R/C=300), the grains are distinct and spherical in shape, with a fairly broad distribution (average diameter $\sim$ 150 Å), and a specific surface area of $\sim$ 550 m^2/g. The cross section of the neck connection between the grains (see Fig. 1) has a size much less than the grain radius. This loose connection between the grains is exhibited in the weak mechanical properties of this aerogel. Another type of colloidal aerogel ($R/C = 200$) can be made, with features similar to its $R/C = 300$ counterpart, except that now, the grain size is more uniform within individual samples (average diameter $\sim$ 120 Å), and the specific surface area is $\sim$ 650 m^2/g.

Polymeric carbon aerogels (high catalyst ratio, $R/C =$ 50), on the other hand, have fewer detectable spherical grains and hence, are morphologically different. For such aerogels, the spherical feature is smeared out as the cross section of the connection between the grains is now on the order of the grain diameter. These highly interconnected grains form a more filamentous structure with characteristic diameters of 70–90 Å. The presence of the filaments in this aerogel results in a more intricate morphology and hence a larger specific surface area ($\sim$ 800 m^2/g).

For the later discussion of the characterization of disorder, we classify disorder by its spatial extent. The disorder associated with granularity is termed *mesoscopic* disorder. Hence, the $R/C = 50$ carbon aerogel is more mesoscopically disordered than the $R/C = 300$ aerogel because the former material has a smaller grain size. Structural defects contained within a grain, such as dangling bonds and other topological disorder, are collectively known as *microscopic* disorder.

III. EXPERIMENTAL DETAILS

The carbon aerogels studied here were derived from the pyrolysis of resorcinol-formaldehyde (RF) aerogels. RF aerogels are, in turn, derived from a process of chemically induced phase separation (sol-gel processing), which is described elsewhere.[1,11] The size and number of RF clusters, the surface area, and the interconnectivity of the RF aerogel can be controlled by varying the R/C molar ratio during the aerogel synthesis. The present study focuses on carbon aerogel samples with $R/C = 50$ (polymeric aerogels) and 300 (colloidal aerogels), respectively. Comparisons in the transport and magnetotransport properties are made with previously studied $R/C = 200$ colloidal carbon aerogels.[6,8,9,12] All measurements were carried out on machined samples of dimension $\sim 8 \times 5 \times 4$ mm^3.

Raman spectroscopy measurements were obtained in a backscattering configuration using a 488-nm excitation (see Ref. 6). A charged coupled device was used to record the Raman spectrum from $\sim$ 1100 to 1800 cm^{-1} for each sample. Transverse magnetic susceptibility measurements were carried out in a Quantum Design magnetometer. Samples were mounted in drinking straws and scanned in a 1-T field in a temperature range of 4–300 K. The 1-T field was chosen in order to obtain a linear response in the susceptibility. For the transport mea-

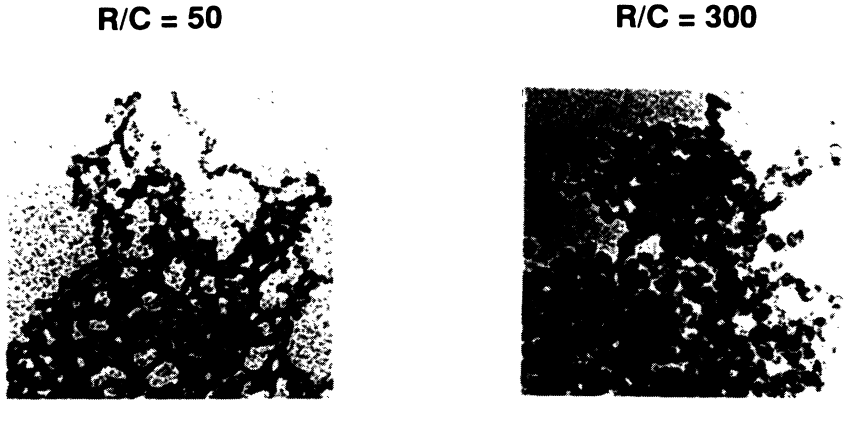

FIG. 1. High-resolution TEM micrographs showing the differences between *polymeric* ($R/C = 50$) and *colloidal* ($R/C = 300$) carbon aerogels.

surements, a four-point contact electrode configuration was used. Joule heating was minimized by keeping the power through the samples below 10^{-7} W at all temperatures. The sample conductivity σ was measured as a function of temperature from 4 to 300 K over a period of 12 h or more to ensure thermal equilibrium. We also measured $\sigma(T)$ from 1.5 to 4 K via natural warming of the samples over a 2-h period to observe the large temperature dependence of the transport properties at these low temperatures.[6,8,12] Transverse magnetoresistance measurements at fixed temperatures in the range of 1.5 to 27 K were conducted in a 15-T Bitter magnet at the Francis Bitter National Magnet Laboratory. All magnetoresistance measurements were taken only after the resistivities of the samples had stabilized at each measurement temperature.

IV. EXPERIMENTAL RESULTS

A. Raman spectroscopy

A typical Raman spectrum for disordered carbons exhibits a Raman-allowed E_{2g_2} peak near 1580 cm^{-1} (designated as the G band). The occurrence of an additional Raman line near 1360 cm^{-1} (the D band) has been attributed to the presence of in-plane disorder. The ratio of the integrated intensity of the disorder-induced D band to that of the G band (i.e., I_D/I_G) is inversely proportional to the in-plane microcrystallite size,[13] L_a. The parameter L_a often serves as a measure of the structural order in disordered carbons.

Figure 2 shows the Raman spectra for low-density carbon aerogel samples with $R/C = 50$, 200, and 300. The line shape of the peak near 1360 cm^{-1} is Lorentzian, while the line near 1580 cm^{-1} has a Breit-Wigner-Fano (BWF) line shape. Table I lists the parameters obtained by fitting the scattered intensity to the BWF line shape given by

$$I(\nu) = \frac{I_0[1 + 2(\nu - \nu_0)/q\Gamma]^2}{1 + [2(\nu - \nu_0)/\Gamma]^2}, \quad (1)$$

where $I(\nu)$ is the frequency-dependent intensity, ν_0 the center phonon position, Γ the full width at half maximum intensity of the Lorentzian line, and $1/q$ a parameter measuring the interactions between the discrete E_{2g_2} mode and a Raman-active continuum ($1/q = 0$ for the Lorentzian line shape).[14]

The in-plane microcrystallite size L_a can be estimated from Knight's empirical formula, $L_a = 44(I_G/I_D)$.[13] The order of magnitude of L_a implies that Raman spectroscopy is most likely probing the dimension of the graphitic filaments within the carbon aerogel grains. That the values of L_a (see Table I) are about the same for all the as-prepared (T_{HT} =1050 °C) samples thus suggests that the structural order internal to the grains of the as-prepared carbon aerogels is approximately the same, irrespective of the density and the R/C molar ratio.

Figure 3 shows that, for the same $R/C = 50$ molar ratio, increasing the heat-treatment temperature (T_{HT}) up to 1800 °C reduces the integrated intensity of the disorder peak, resulting in a larger L_a (see Table I). This behavior is also observed in the $R/C = 300$ samples and is consistent with the idea that heat treatment anneals the microscopic disorder and induces in-plane order development in carbon aerogels.[7,8]

B. Electrical conductivity

In Fig. 4, showing a semilogarithmic plot of the conductivity (σ) versus temperature (T), a sharp temperature dependence below 30 K can be observed for all the low-density samples. Further emphasized in the log-log plot of σ versus T (inset to Fig. 4), the strong temperature dependence of $\sigma(T)$ at low T is indicative of a strongly localized system. In particular, the low-density $R/C = 50$ sample below 5 K has a resistance that falls off by six orders of magnitude over a 1 K temperature

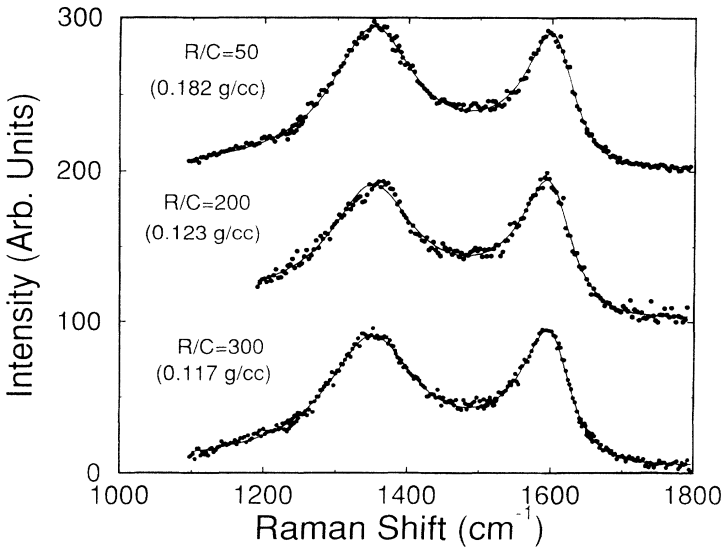

FIG. 2. Raman spectra of three low-density as-prepared carbon aerogel samples with various R/C molar ratios, showing the disorder-induced (~1360 cm^{-1}) and the Raman-active (~1580 cm^{-1}) lines. Solid lines are the fits of the data to Eq. (1). (Data for the $R/C = 200$ sample were obtained from Ref. 6.)

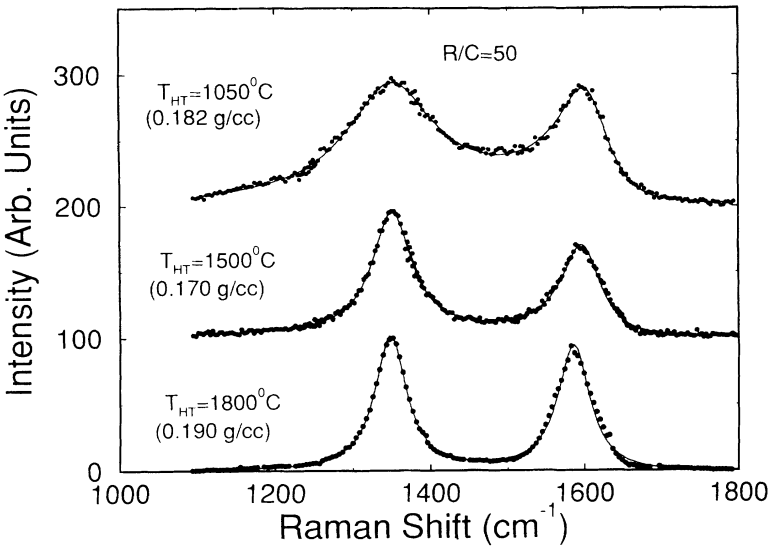

FIG. 3. Raman spectra of three low-density carbon aerogels with $R/C = 50$ and various heat-treatment temperatures. The integrated intensity of the disorder-induced peak relative to the Raman-active line is reduced as the heat-treatment temperature reaches 1800 °C. Solid lines are the fits to Eq. (1).

range. Below 4 K, its resistance is on the order of gigaohms, making low-temperature measurements on this sample very difficult. This sharp decrease in conductivity at low temperatures has been observed in previous studies of carbon aerogels.[6,8,9,12] The behavior of $\sigma(T)$ for the low-density $R/C = 50$ samples is similar to that of the low-density $R/C = 200$ and 300 aerogels. However, the low-temperature conductivity for $R/C = 50$ samples tends to be more strongly temperature dependent than for the $R/C = 200$ and 300 samples, for a fixed mass density ρ_m. The conductivity of all the high-density samples shows a weaker temperature dependence.

We have observed an $\exp(-\sqrt{T_0/T})$ temperature dependence in the conductivity, as shown in the semilogarithmic plot of σ vs $1/\sqrt{T}$ in Fig. 5. Linear fits of the data to the semilogarithmic plots of σ vs $(1/T)^p$ (where $p = 1, 1/2, 1/3, 1/4$), as would be done in an analysis for variable-range hopping systems (see Sec. V), resulted in $p = 1/2$ giving the best linear fit. The $p = 1/2$ dependence in Fig. 5 is universal for all the samples studied and is effective only at very low temperatures ($T < 10$ K), especially for the low-density samples. The $p = 1/2$ dependence is suggestive of a Coulomb-gap variable-range hopping mechanism (see Sec. V). We have conducted magnetoresistance studies to corroborate this identification of the transport mechanism, the results of which are discussed in Sec. V. The aforementioned exponential temperature behavior of σ has also been observed in granular metals (GM's).[15]

Although no low-temperature ($T < 4$ K) data are available for the low-density $R/C = 50$ heat-treated (T_{HT} =1800°C) sample, the transport mechanism associated with the $p = 1/2$ behavior is likely to apply to this sample at low temperatures as well, since its conductivity follows a trend similar to that of the as-prepared low-density $R/C = 200$ and 300 samples.

The large range of magnitudes of the conductivity in Fig. 5 also suggests that the grain size plays a role in the transport, since by increasing the R/C molar ratio, the electrical conductivity increases dramatically.

C. Magnetic susceptibility

Figure 6 shows the magnetic susceptibility $\chi(T)$ as a function of $1/T$ for high- and low-density carbon aerogels. In the low-temperature regime, the data can be fit to a Curie-like behavior given by

$$\chi = \chi_0 + \frac{N\mu_B^2}{3k_BT} \ . \tag{2}$$

TABLE I. Raman parameters for carbon aerogels (see text).

R/C[a]	50	50	50	50	200	200	300	300	300	300
Density (g/cm^3)	0.182	0.672	0.170	0.190	0.123[b]	0.670[b]	0.117	0.801	0.78	0.66
T_{HT} (°C)	1050	1050	1500	1800	1050	1050	1050	1050	1500	1800
ν_{1360} (cm^{-1})	1350	1355	1350	1348	1349	1350	1350	1354	1354	1349
Γ_{1360} (cm^{-1})	141	128	63	50	143	123	150	133	62	59
ν_{1580} (cm^{-1})	1609	1614	1599	1586	1604	1607	1604	1613	1599	1596
Γ_{1580} (cm^{-1})	82	77	61	50	86	73	83	77	62	61
I_{1360}/I_{1580}	1.8	1.8	1.4	1.1	1.5	1.6	1.7	2.0	1.4	0.97
L_a (Å)	24	24	31	40	29	27	25	23	31	45

[a]Resorcinol/catalyst molar ratio.
[b]Data from Ref. 6.

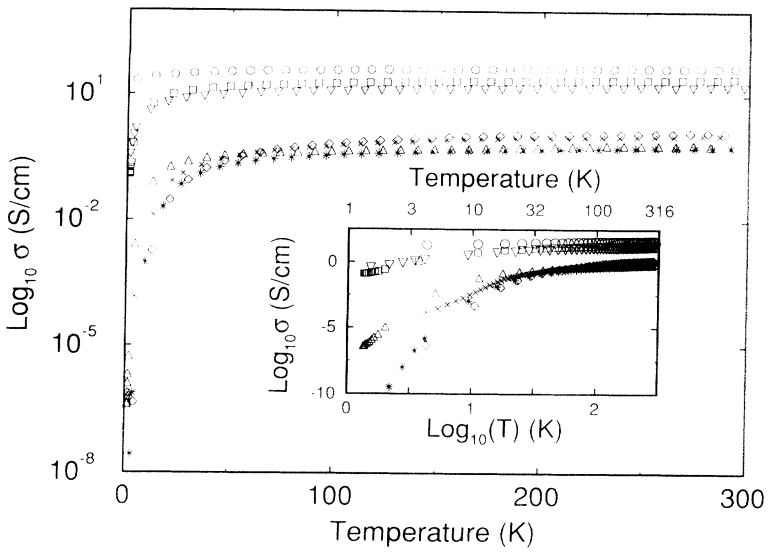

FIG. 4. Plot of $\log_{10}\sigma$ versus T for the carbon aerogels studied. The inset shows the corresponding $\log_{10}$-$\log_{10}$ plot of σ versus T, thereby emphasizing the low T behavior. ○: $R/C = 300$, ρ_m=0.801 g/cc; □: $R/C = 50$, ρ_m=0.672 g/cc; ▽: $R/C = 200$, ρ_m=0.670 g/cc; △: $R/C = 300$, ρ_m=0.117 g/cc; ∗: $R/C = 200$, ρ_m=0.123 g/cc; ◇: $R/C = 50$, ρ_m=0.182 g/cc; ×: $R/C = 50$, ρ_m=0.190 g/cc; T_{HT}=1800 °C. (Data for the $R/C = 200$ sample were obtained from Ref. 6.)

The number of spins per gram is denoted by N, μ_B is the Bohr magneton, k_B is Boltzmann's constant, and χ_0 is the temperature-independent diamagnetic offset at high temperatures, observable in all the samples studied and typical of graphitic materials. The peak at high temperatures in the susceptibility curves for the as-prepared low-density $R/C = 50$ and 300 samples in Fig. 6 is due to the presence of oxygen impurity in the magnetometer, but this peak does not disguise the observed linear $1/T$ dependencies at low temperatures. To get a measure of the microscopic disorder in these aerogel systems, we choose to look at the susceptibility on the per-unit-weight basis and not per-unit-volume basis because dangling bonds and other structural defects are present only in the grains and not in the mesopores. Generally, the samples with $R/C = 50$ exhibit a stronger low-temperature dependence, and hence a larger number of unpaired spins per gram (see Table II) than their $R/C = 200$ and 300 counterparts for the same sample density, suggesting that these samples are more microscopically disordered.

By comparing the conductivities and the susceptibilities for all the carbon aerogel samples, we can obtain the relationship between the microscopic disorder and the observed conductivities. On the one hand, we see from Fig. 5 and Table II that the as-prepared low-density $R/C = 50$ sample, with the highest value of N (and hence the most microscopic disorder), has the lowest conductivity among all the carbon aerogel samples studied. On the other hand, comparing the as-prepared high-density $R/C = 50$ and the heat-treated low-density $R/C = 50$ samples, we observe that the conductivity decreases as the microscopic disorder (N) decreases. These contradictory trends suggest that there is no direct correlation between the observed microscopic disorder and the sample conductivity.

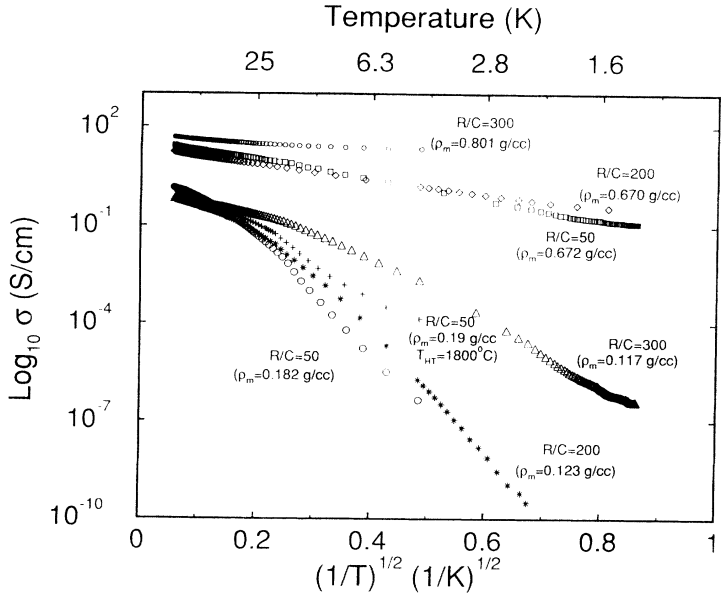

FIG. 5. Semilogarithmic plot of $\log_{10}\sigma$ versus $(1/T)^{1/2}$ of the carbon aerogel samples in Fig. 4.

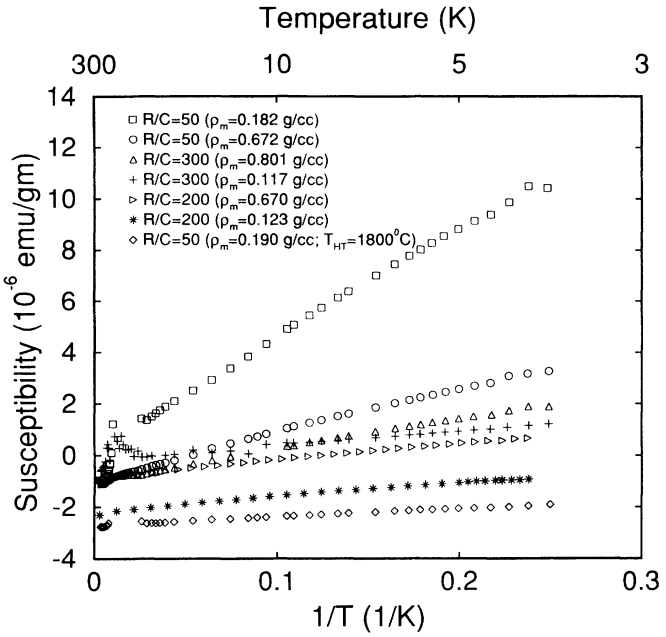

FIG. 6. Susceptibility versus $1/T$ for high- and low-density carbon aerogels with different R/C ratios. (Data for the $R/C = 200$ sample were obtained from Ref. 6.)

D. Transverse magnetoresistance

The transverse magnetoresistance was measured at temperatures ranging from 1.5 to 27 K for the high-density $R/C = 50$ and the low-density $R/C = 50$ and 300 as-prepared samples. Figures 7(a)–(c) show the magnetoresistance $[\rho(H) - \rho(0)]/\rho(0) \equiv \Delta\rho/\rho$ as a function of magnetic field (H) for various values of measurement temperature for the low-density ($\rho_m = 0.117$ g/cc) $R/C = 300$, the low-density ($\rho_m = 0.182$ g/cc) $R/C = 50$ and the high-density ($\rho_m = 0.672$ g/cc) $R/C = 50$ samples, respectively. The magnetoresistance for all the samples studied is positive and large in comparison with other disordered carbon materials.[16] Similar behavior in $\Delta\rho/\rho$ as a function of field has been observed for the $R/C = 200$ samples.[9] The magnetoresistance is temperature dependent, with the largest $\Delta\rho/\rho$ occurring at low temperatures ($T < 4$K).

In Fig. 8, in which $\Delta\rho/\rho$ is plotted vs H at 4.3 K for both high- and low-density aerogels with various R/C molar ratios, we see that $\Delta\rho/\rho$ is more a function of sample density than R/C ratio. This implies that the transport mechanism inherent to the polymeric and colloidal aerogels is related to the packing ratio of the grains. We also observe that the low-density $R/C = 50$ aerogel exhibits the largest $\Delta\rho/\rho$ (121% at 15 T). This is consistent with the large temperature dependence of the conductivity exhibited by this sample at low temperature in the semilogarithmic plot of $\sigma(T)$ versus T (see Fig. 4). The magnetoresistance and conductivity data suggest that of all the samples studied, this low-density $R/C = 50$ sample is the most mesoscopically disordered.

The transverse magnetoresistance follows a quadratic form at low fields as shown in Fig. 9, in which $\Delta\rho/\rho$ is plotted vs H^2 for the high-density $R/C = 50$ sample in Fig. 7(c). This quadratic behavior was observed in all of the three samples studied and becomes suppressed (saturated) at high magnetic fields, with the saturation field decreasing with decreasing temperature. Further discussion of the temperature and the magnetic field dependences of the magnetoresistance is given in Sec. V.

V. DISCUSSION

Fung *et al.*[9] have observed an $\exp[-(T_0/T)^p]$ temperature dependence ($p = 1/2$) in the conductivity of $R/C = 200$ colloidal carbon aerogels. They attributed this behavior to variable range hopping (VRH) in a Coulomb-gap in the density of states. As noted in Sec. IV B, we also observed the same $p = 1/2$ behavior in the conductivity data for our colloidal and polymeric carbon aerogels, which is consistent with a Coulomb-gap VRH mechanism. It is noted that the determination of the p value by plotting $\log_{10}\sigma$ vs $(1/T)^p$ for different p values is somewhat ambiguous because of the finite temperature range for which the $(1/T)^{1/2}$ plot is linear. It is also possible that the observed $p = 1/2$ behavior is not due to the CGVRH mechanism. Since the CGVRH model also predicts a unique temperature dependence for the magnetoresistance, we can confirm the findings from our conductivity study by measuring the magnetoresistance as a function of temperature.

The presence of a positive magnetoresistance is suggestive of a hopping conductivity mechanism. When a Coulomb gap is present in the density of states, the magnetoresistance in the VRH regime is given by[10]

$$\ln\left[\frac{\rho(H)}{\rho(0)}\right] = t\left(\frac{\xi}{\lambda}\right)^4\left(\frac{T_0}{T}\right)^{3p} \equiv MH^2, \qquad (3)$$

where $\lambda \equiv \sqrt{c\hbar/eH}$ is the magnetic length, ξ the local-

TABLE II. Susceptibility parameters for carbon aerogels.

R/C[a]	50	50	50	200	200	300	300
Density (g/cm^3)	0.182	0.672	0.190	0.123[b]	0.670[b]	0.117	0.801
T_{HT} (°C)	1050	1050	1800	1050	1050	1050	1050
N (10^{19} spins/g)	21	8.8	1.6	2.8	3.3	2.3	5.9
χ_0 (10^{-6} emu/g)	-2.1	-1.3	-0.27	-2.3	-1.0	-0.71	-1.1

[a]Resorcinol/catalyst molar ratio.
[b]Data from Ref. 6.

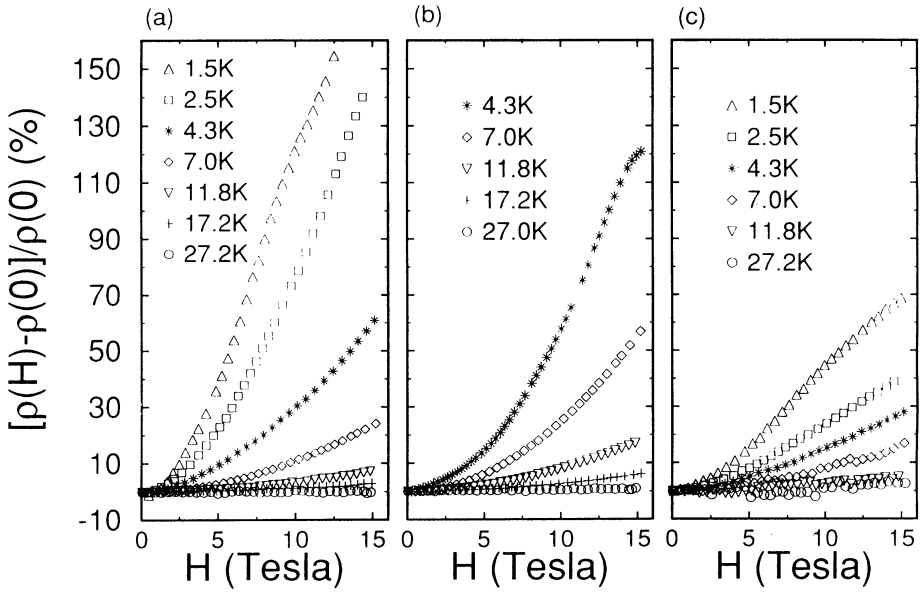

FIG. 7. $[\rho(H) - \rho(0)/\rho(0)]$ versus H for carbon aerogels of (a) low density ($\rho_m = 0.117$ g/cc) and $R/C = 300$, (b) low density ($\rho_m = 0.182$ g/cc) and $R/C = 50$, and (c) high density ($\rho_m = 0.672$ g/cc) and $R/C = 50$, at various measurement temperatures.

ization length, T_0 the same characteristic temperature as in Eq. (6), $p = 1/2$ and $t = 0.0015$ for a three-dimensional system. Equation (3) is valid in the weak field regime, i.e., for $\lambda \gg \xi$. By fitting the low-field linear regime in a plot of $\ln[\rho(H)/\rho(0)]$ versus H^2, a value for M as a function of T can be obtained. A log-log plot of M vs T gives the p dependence in Eq. (3). Thus, an observed value of $p = 1/2$ would be consistent with both the observed conductivity and the CGVRH mechanism.

Figure 10 shows a log-log plot of the slope M versus T for the three measured carbon aerogel samples. The resultant slope corresponds to the value for $3p$ in Eq. (3). For both the high-density $R/C = 50$ sample and the low-density $R/C = 300$ sample, the data in Fig. 10 show that $p \sim 0.5$. Since the magnetoresistance for the low-density $R/C = 50$ sample could not be measured at very low temperatures, no good estimate for p could be obtained for this sample. The approximate value of $p = 0.7$ indicated by the four points in Fig. 10 is, therefore, an overestimate for p for this sample, since the onset of the $p = 1/2$ behavior occurs around 4 K for this sample. The value of $p = 1/2$ obtained from Fig. 10 confirms the value of p obtained from the plot of $\log_{10}\sigma$ versus $1/\sqrt{T}$ in Fig. 5, and suggests that CGVRH is indeed possible in polymeric as well as colloidal carbon aerogels.

It is interesting to understand how VRH is possible in carbon aerogels with varied morphologies. We do this by first reviewing how the CGVRH mechanism manifests itself in a disordered system and then adapting this mechanism to the carbon aerogel system.

In an amorphous system, as the temperature is lowered, the conduction mechanism is by hopping between states with energies lying close to the Fermi level. For a nonvanishing constant density of states at the Fermi

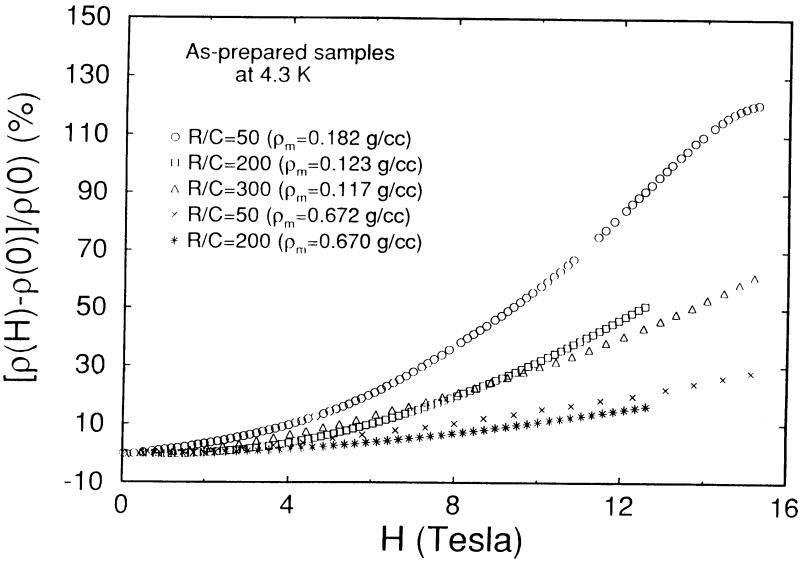

FIG. 8. $[\rho(H) - \rho(0)/\rho(0)]$ versus H for carbon aerogel samples with different densities and R/C ratios at 4.3 K. (Data for the $R/C = 200$ sample were obtained from Ref. 6.)

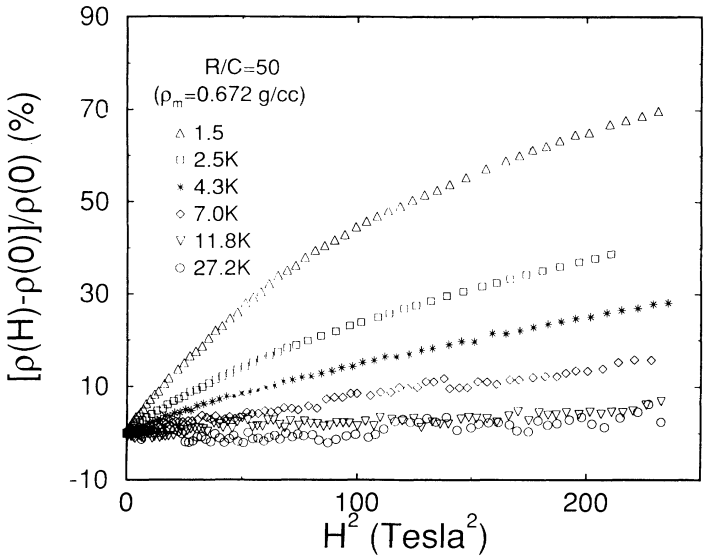

FIG. 9. $[\rho(H) - \rho(0)/\rho(0)]$ versus H^2 for the $R/C = 50$ sample with $\rho_m = 0.672$ g/cc.

level, the conductivity follows Mott's law[17]

$$\sigma = \sigma_0 \exp[-(T_0/T)^p] \tag{4}$$

with $p = 1/(n+1)$ for an n-dimensional system. The hopping distance is temperature dependent, unlike the case of nearest-neighbor (NN) hopping; hence the Mott's law behavior is referred to as VRH conduction. When electron-electron interactions are taken into account, Efros and Shklovskii[10,18] have shown that a quasigap appears in the density of states at the Fermi level, and that the resulting conductivity exhibits a CGVRH conduction mechanism given by

$$\sigma = \sigma_0 \exp[-(T_0/T)^{1/2}], \tag{5}$$

where

$$T_0 = \frac{\beta e^2}{\kappa k_B \xi}, \tag{6}$$

with κ being the dielectric constant, ξ the localization length, k_B Boltzmann's constant, and $\beta = 2.8$ for a three-dimensional system.[10] This $p = 1/2$ dependence has been observed in both amorphous semiconductors[19] and granular metals (GM's),[15] although the origin of this dependence is not well established in the latter system.

The GM material consists of metallic grains of some average size d, randomly dispersed in an insulating matrix with an average separation s between the grains. The aerogel system is similar to the GM material in its structure of grains and pores. However, unlike the GM, the grains in the carbon aerogel system are necessarily closely connected in order to maintain the solid structure, resulting in a granular separation s much less than the grain size d.

Various studies have been done on the transport properties of GM's in order to explain the $p = 1/2$ dependence of the conductivity. Studies have shown that this dependence was possible under the assumption of s/d =constant.[15,20] However, this assumption is not always experimentally verified in all systems, including carbon aerogels. For uncorrelated distributions of s and d (with $s \sim d$), the critical path method[21,22] results in an approximate $p = 1/2$ dependence in the intermediate regime between VRH and tunneling.

The idea of VRH in GM's has not been widely adopted since the electron wave function decays rapidly in the insulating gap between neighboring grains. The study of Fung *et al.*[9] has addressed the issue of how VRH could occur in carbon aerogels with their connected-grain morphology. The grains and the insulating gaps between the grains can present barriers of height ϕ_d and ϕ_s, respectively. If the wave function decays rapidly across the gaps and $s \sim d$, then NN hopping should dominate over VRH because the probability of locating an electron beyond a NN grain decreases almost exponentially with distance. However, because of the fluctuations in the grain energy

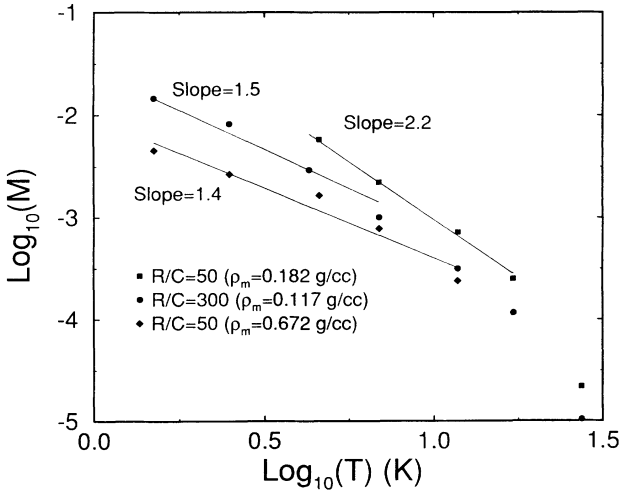

FIG. 10. Log_{10}-log_{10} plot of M in Eq. (3) versus T for three as-prepared carbon aerogel samples (see text). The slopes of the curves in this figure give the values of $3p$ in Eq. (3).

due to the surrounding random disorder potential (see below), the wave function decay over the grain could be larger than that between the grains, especially for $s \ll d$, as is the case for carbon aerogels.[9] When an image force is taken into account, ϕ_s could be significantly lowered, further reducing the wave function decay in the gaps between neighboring grains, leaving ϕ_d as the only effective means for carrier localization.

Adkins[23] proposed that fluctuations in the charging energy E_c of the grains are caused by a random disorder potential near each grain. The charging energy is defined as the energy required to move a charge from infinity onto a neutral conducting grain and is given by

$$E_c \sim \frac{e^2}{\kappa d}, \tag{7}$$

where e is the charge, κ the effective dielectric constant of the medium through which the charge is moving, and d the size of the grain. As E_c can only change in the presence of the random disorder potential by an amount of $2E_c$ without discharging, the energy of the system as a whole forms a band of localized states between $E_F \pm 2E_c$, where E_F is the Fermi energy. The average effective barrier height ϕ_d is then on the order of the fluctuations of E_c, i.e.,

$$\phi_d \sim 2E_c \ . \tag{8}$$

With the introduction of the fluctuations in the grain energy, we can replace the localization length ξ with an effective wave function decay length ($\chi_{\rm eff}^{-1}$) within the grains, given as a function of the effective barrier height ϕ_d,

$$\chi_{\rm eff} = \sqrt{\frac{2m^*\phi_d}{\hbar^2}} \tag{9}$$

in which m^* is the effective mass of the carriers.

From the above discussion, the finite grain size does not prevent one from observing VRH in the Coulomb-gap regime. Fung *et al.*[9] suggested that β (=2.8) is unchanged in Eq. (6) for the aerogel morphology. From the $p = 1/2$ dependences in the magnetoresistance and the conductivity data, the CGVRH mechanism, as previously applied to explain the low-temperature conduction in carbon aerogel samples with $R/C = 200$, is seen to be retained, despite changes of grain size ranging from ~70 to 150 Å.

Table III lists values of T_0, κ, $\chi_{\rm eff}^{-1}$ and m^* as obtained from the CGVRH model. These values were obtained from experiment as follows. A fit of the conductivity curves (Fig. 5) to Eq. (5) resulted in values of T_0. The curves were fit in a temperature range corresponding to an onset of the $p = 1/2$ behavior at low temperature. The T_0 values were then used along with the values of the slope M [from Eq. (3)] to obtain $\chi_{\rm eff}$. The values for κ were then obtained from Eq. (6) and used, along with $\chi_{\rm eff}$, to procure values of m^* from Eq. (9). The lack of low-temperature data for the low-density as-prepared $R/C = 50$ sample resulted in an underestimation of T_0, and hence the unphysically small values of m^* in Table III. Since the grain size d is not uniform within the $R/C = 50$ aerogel, a range of possible values for m^* results, as shown in Table III. Previous work[9] done on $R/C = 200$ aerogels has shown that an average effective mass of $m^* \simeq 0.1m_0$ has consistently resulted in reasonable grain sizes. Using this value of m^* results in the grain sizes listed in parentheses in Table III. These grain sizes, as obtained from the CGVRH model, are consistent with the average grain sizes measured with high-resolution TEM.[24]

Table III suggests that the wave function decay length ($\chi_{\rm eff}^{-1}$) is correlated with the mass density. The high-density samples have larger $\chi_{\rm eff}^{-1}$ than the low-density samples, in accordance with the closer packing of the grains and hence the observed increase in κ. This trend in $\chi_{\rm eff}^{-1}$ has been previously observed in $R/C = 200$ aerogels with varied densities.[9] We can estimate the hopping distance, given approximately by $\chi_{\rm eff}^{-1}(T_0/T)^{1/2}$, and compare this with the grain sizes obtained using an effective mass of $0.1m_0$. From Fig. 5, the $p = 1/2$ dependence of $\log_{10}\sigma$ is valid for $T < 20$ K and $T < 16$ K for the high-density $R/C = 50$ and the low-density $R/C = 300$ carbon aerogels, respectively. Using values for T_0 and $\chi_{\rm eff}^{-1}$ from Table III, we obtain minimum hopping distances of 149 Å and 315 Å for the $R/C = 50$ and 300 samples, respectively. These distances are approximately two times the average grain sizes, suggesting that not only is VRH possible, but that the carbon grains, and not the dangling bonds, act as localization sites. This is further corroborated by the magnetic susceptibility results as discussed below.

Despite the smearing of the grains in the $R/C = 50$ samples, the magnitude of L_a in Table I suggests that

TABLE III. CGVRH parameters for carbon aerogels.

R/C[a]	50	50	200	200	300
Density (g/cm^3)	0.182	0.672	0.123[b]	0.670[b]	0.117
$T_{\rm HT}$(°C)	1050	1050	1050	1050	1050
T_0 (K)	1849	45	2100	30	502
κ	6.5	105.4	6	110	16.6
d (Å)	70–90	70–90 (70)	120[c]	120[c]	150 (160)
$\chi_{\rm eff}^{-1}$ (Å)	39	99	35	140	56
m^* (units of m_0)	0.04–0.05	0.10–0.13	0.08	0.09	0.10

[a]Resorcinol/catalyst molar ratio.
[b]Data from Ref. 6.
[c]Grain size based on m^*=$0.1m_0$.

the structure internal to a grain in carbon aerogels is independent of both the R/C ratio and the mass density. The magnitude of L_a is in good agreement with the size of the carbon filaments within the grains, as observed by high-resolution TEM.[24] With heat treatment, L_a increases slightly and the microscopic disorder in the system also becomes annealed, both effects being shown by the Raman scattering measurements.

The specific surface area increases with decreasing R/C, and this manifests itself in a large concentration of unpaired spins, as can be seen from the values of N in Table II. It is noted that the increase in the specific surface areas (SSA's) from $R/C = 300$ to 50, quoted in Sec. II from results of gas adsorption measurements, could not account for the much larger increase in N in the low-density $R/C = 50$ carbon aerogel, probably because part of the actual SSA is inaccessible to the vapor used in the adsorption measurement. However, the increase in N can be explained by the SSA increase calculated from the average grain sizes listed in parentheses in Table III, suggesting that the grain size calculated from the CGVRH model is indeed correct, and that the SSA available for charge storage might be more accurately measured by transport and capacitance measurements than by adsorption methods.

There is no clear correlation between the spin concentration (as denoted by N) and the conductivity. For example, in Table II, the number of unpaired spins per gram for the low-density heat-treated (T_{HT} =1800 °C) $R/C = 50$ aerogel, which also exhibits a strong localization behavior (see Sec. IV B), is smaller than that for the high-density as-prepared $R/C = 50$ aerogel. From Fig. 5, the high-density as-prepared $R/C = 50$ sample has a larger conductivity than the low-density heat-treated $R/C = 50$ sample, seemingly suggesting that the conductivity increases with increasing microscopic disorder. However, by comparing the low-density as-prepared and heat-treated $R/C = 50$ aerogels, we observe that the conductivity now decreases with increasing microscopic disorder. This suggests that the low-temperature conduction mechanism is more related to the density than to the unpaired spin concentration, since with increasing density, there is always an increase in the conductivity. Since the density is correlated with the packing ratio of the grains, it is likely that the grains, rather than the defects, act as the carrier localization sites in the CGVRH process.

For the low-density $R/C = 200$ and $R/C = 300$ as-prepared samples, although the mass density and the unpaired spin concentration in both systems are similar (i.e., equal microscopic disorder), their conductivities are very different. The only variable is the grain size. Once again, the unpaired spins do not correlate with the observed conductivities, thus further supporting our CGVRH model in which the grains are the localization sites and the grain size (i.e., the granularity or mesoscopic disorder) is an important parameter in determining the sample resistance.

The colloidal and polymeric aerogels not only differ in grain size but also in the distinction of individual grains. Despite the morphological differences, we see that colloidal and polymeric aerogels exhibit similar transport behavior. This tends to suggest that polymeric and colloidal aerogels do not represent two structural extremes, as also pointed out in a previous high-resolution TEM study.[5] The synthesis process for both types of aerogels should follow similar pathways, except that under high catalyst concentrations (i.e., $R/C = 50$), the process of cluster (grain) formation is short lived because growing RF chains are quickly being connected to other RF chains nearby, resulting in smaller grain sizes in the polymeric carbon aerogels. Though obscured in a high-resolution TEM micrograph by the presence of highly branched carbon filaments, these small grains should constitute the insulated conducting regions (and localization sites for charge carriers) in polymeric aerogels, as suggested by the transport results. Finally, it is worth mentioning that the structural links between neighboring grains are not necessarily electrically conducting. As such, more nonconducting regions (defects) would be expected in polymeric carbon aerogels, leading to lower electrical conductivity at a given density as compared to colloidal carbon aerogels. These data are still consistent with the superior mechanical properties of polymeric carbon aerogels since the nonconducting defects can support mechanical loads.[25]

VI. CONCLUSION

By adjusting the molar ratio of the resorcinol and catalyst concentrations during the carbon aerogel synthesis, the grain size can be varied from approximately 70 to 150 Å. The increased surface area presented by the aerogels with the smaller grain size leads to more defects in the system. These defects can be seen in an increase in the unpaired spin concentration, but the change cannot be consistently correlated with the conductivity data. Results show that the variation in grain size does not affect the transport mechanism, which is seen to be variable-range hopping in a Coulomb gap in the density of states. The mass density and the R/C molar ratio play a more important role in the electrical conductivity than the concentration of unpaired spins, indicating that the conduction mechanism is dominated by the carriers localized by the grains and not by the carriers trapped in the defect states. Since polymeric aerogels also exhibit the same variable-range hopping conduction mechanism as colloidal aerogels, the morphological structure of carbon aerogels does not seem to be an important factor in their transport behavior, as long as the conducting elements are electrically insulated from each other and effectively localize the carriers. The grain size and the mass density can thus be treated as useful parameters for the characterization of electrical transport in carbon aerogels.

ACKNOWLEDGMENTS

We would like to thank J. Sod for his help in the analysis of the Raman data. The M.I.T. authors grate-

fully acknowledge support from Lawrence Livermore National Laboratory subcontract No. B130530. The aerogel synthesis was performed under the auspices of the U.S. Department of Energy by Lawrence Livermore National Laboratory under Contract No. W-7405-ENG-48, with financial support from the Office of Basic Energy Sciences, Division of Advanced Energy Project.

[1] For a review, see Mater. Res. Bull. **15**, 19 (1990).
[2] R. W. Pekala, C. T. Alviso, F. M. Kong, and S. S. Hulsey, J. Non-Cryst. Solids **145**, 90 (1992).
[3] R. W. Pekala and F. M. Kong, J. Phys. (Paris) Colloq. Suppl. **50**, C4-33 (1989).
[4] R. W. Pekala, C. T. Alviso, and J. D. LeMay, in *Chemical Processing of Advanced Materials*, edited by L. Hench and J. West (Wiley, New York, 1992), p. 671.
[5] G. C. Ruben, R. W. Pekala, T. M. Tillotson, and L. W. Hrubesh, J. Mater. Sci. **27**, 4341 (1992).
[6] A. W. P. Fung, Z. H. Wang, K. Lu, M. S. Dresselhaus, and R. W. Pekala, J. Mater. Res. **8**, 1875 (1993).
[7] J. J. Chen (private communication).
[8] G. A. M. Reynolds, Z. H. Wang, M. S. Dresselhaus, A. W. P. Fung, and R. Pekala, Phys. Rev. B **49**, 15 027 (1994).
[9] A. W. P. Fung, Z. H. Wang, M. S. Dresselhaus, G. Dresselhaus, R. W. Pekala, and M. Endo, Phys. Rev. B **49**, 17 325 (1994).
[10] B. I. Shklovskii and A. L. Efros, *Electronic Properties of Doped Semiconductors* (Springer-Verlag, New York, 1984).
[11] L. L. Hench and J. K. West, Chem. Rev. **90**, 33 (1990).
[12] M. Hosoya, G. Reynolds, M. S. Dresselhaus, and R. W. Pekala, J. Mater. Res. **8**, 811 (1993).
[13] D. S. Knight and W. B. White, J. Mater. Res. **4**, 385 (1992).
[14] M. V. Klein, in *Light Scattering in Solids I*, edited by M. Cardona, Topics in Applied Physics Vol. 8 (Springer-Verlag, New York, 1983), p. 147.
[15] P. Sheng, B. Abeles, and Y. Arie, Phys. Rev. Lett. **31**, 44 (1973).
[16] P. Delhaès, in *Chemistry and Physics of Carbon*, edited by P. L. Walker, Jr. (Marcel Dekker, New York, 1971), Vol. 7, p. 193.
[17] N. F. Mott, J. Non-Cryst. Solids **1**, 1 (1968).
[18] A. L. Efros and B. I. Shklovskii, J. Phys. C **8**, L49 (1975).
[19] H. Tokumoto, R. Mansfield, and M. J. Lea, Solid State Commun. **35**, 961 (1980).
[20] B. Abeles, P. Sheng, M. D. Coutts, and Y. Arie, Adv. Phys. **24**, 407 (1975).
[21] E. Šimánek, Solid State Commun. **40**, 1021 (1981.)
[22] P. Sheng and J. Klafter, Phys. Rev. B **27**, 2583 (1983).
[23] C. J. Adkins, J. Phys. C **20**, 235 (1987).
[24] R. W. Pekala, S. T. Mayer, J. L. Kaschmitter, and F. M. Kong, in *Proceedings of the International Symposium on Advances in Sol-Gel Processing and Applications*, edited by Yosry A. Attia (Plenum, New York, in press).
[25] R. W. Pekala, C. T. Alviso, and J. D. LeMay, J. Non-Cryst. Solids **125**, 67 (1990).

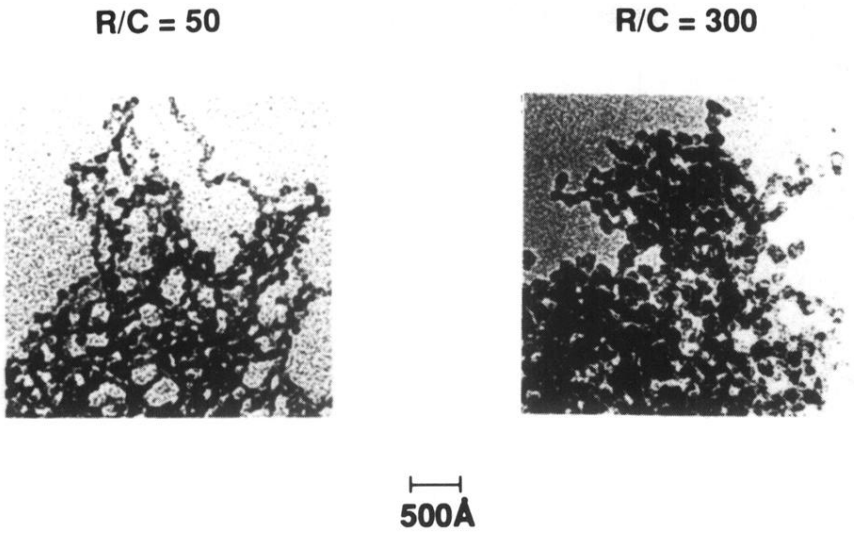

FIG. 1. High-resolution TEM micrographs showing the differences between *polymeric* ($R/C = 50$) and *colloidal* ($R/C = 300$) carbon aerogels.